

MIT Open Access Articles

*Optimization of THz Wave Coupling into
Samples in DNP/NMR Spectroscopy*

The MIT Faculty has made this article openly available. **Please share** how this access benefits you. Your story matters.

Citation: Barnes, Alexander et al. "Optimization of THz wave coupling into samples in DNP/NMR spectroscopy." Proceedings of the 2010 IEEE International Conference on Millimeter and Terahertz Waves: 1-3. © Copyright IEEE

As Published: <http://dx.doi.org/10.1109/ICIMW.2010.5612956>

Publisher: Institute of Electrical and Electronics Engineers (IEEE)

Persistent URL: <http://hdl.handle.net/1721.1/73044>

Version: Final published version: final published article, as it appeared in a journal, conference proceedings, or other formally published context

Terms of Use: Article is made available in accordance with the publisher's policy and may be subject to US copyright law. Please refer to the publisher's site for terms of use.



Optimization of THz Wave Coupling into Samples in DNP/NMR Spectroscopy

Emilio A. Nanni^a, Alexander B. Barnes^b, Yoh Matsuki^b, Paul P. Woskov^a, Björn Corzilius^b, Robert G. Griffin^b and Richard J. Temkin^a

^aPlasma Science and Fusion Center, MIT, Cambridge, MA, 02139, USA

^bFrancis Bitter Magnet Laboratory, MIT, Cambridge, MA, 02139, USA

Abstract— High power millimeter wave and terahertz sources are used in DNP/NMR spectroscopy to greatly enhance the NMR signal. A key issue is the efficient coupling of the source power to the sample. We present HFSS calculations showing that the MIT 250 GHz DNP/NMR system provides a B_1 value of $13 \mu\text{T}/\text{W}^{1/2}$. The simulation shows the importance of the diffraction of radiation passing through the RF coil, leading to non-uniform illumination of the sample. A simple single pass model yields insight into the origin of the observed B_1 value. Methods of optimizing the B_1 value are described.

I. INTRODUCTION AND BACKGROUND

Dynamic nuclear polarization (DNP) yields drastic gains in sensitivity of nuclear magnetic resonance (NMR) experiments by irradiating electron paramagnetic resonance (EPR) manifolds with high-power millimeter radiation.¹ Sensitivity enhancements of 50-200 are routine and are expected to have a profound impact on structural studies of disease related biomolecules such as membrane proteins and amyloid fibrils. Signal enhancements in DNP experiments are dependent on the distribution and intensity of the B_1 field throughout the sample. The B_1 field consists of the component of the magnetic field that is orthogonal to the main magnetic field B_0 and is oscillating at a frequency, $f_1 = \gamma_e B_0 / 2\pi$, that is resonant with the electron spins. For this experiment, $B_0 = 8.9 \text{ T}$ and $f_1 = 250 \text{ GHz}$. In magic angle spinning (MAS) DNP experiments, the B_1 field is generated from millimeter waves produced from an external source coupled to the sample via overmoded waveguides and quasi-optical mirror units.^{2,3} The millimeter waves are launched as a Gaussian beam into the sample cavity perpendicular to the axis of symmetry for the sample holder, as shown in Figure 1. However, due to the constraints imposed by the system, i.e. a cylindrical sapphire rotor, directionality of the millimeter wave and RF magnetic field, a large high voltage RF pickup coil and the highly overmoded nature of the sample and cavity, designing an efficient coupling mechanism for millimeter wave power into the sample has proved very challenging. This paper presents two models used to analyze and predict the performance of millimeter wave coupling in DNP experiments. The first model presented is the result of HFSS simulations of the entire sample chamber. The second method is a single pass model based on Gaussian beam propagation and Fresnel diffraction that allows for quick inspection of the sample irradiation cavity or probe.

II. HFSS MODEL

The dielectric constant of the sample must be known in order to accurately model the millimeter wave coupling. The DNP experiments of interest are performed at 80 Kelvin using a

sample dissolved in a mixture of glycerol/ice. The dielectric constant was measured under these conditions at 140 GHz; the real part of which was 3.5 with a loss tangent of 0.005. Measurements on ice at low temperatures show that the real part of the dielectric constant varies very slowly with frequency, while the imaginary part increases with frequency.^{4,5} To obtain the dielectric constant at 250 GHz, we scale the 140 GHz values, keeping the real part constant (3.5) and scaling the loss tangent linearly with frequency (0.009). The general conclusions of this study are not critically dependent on the exact values of these parameters, which may vary with sample content.

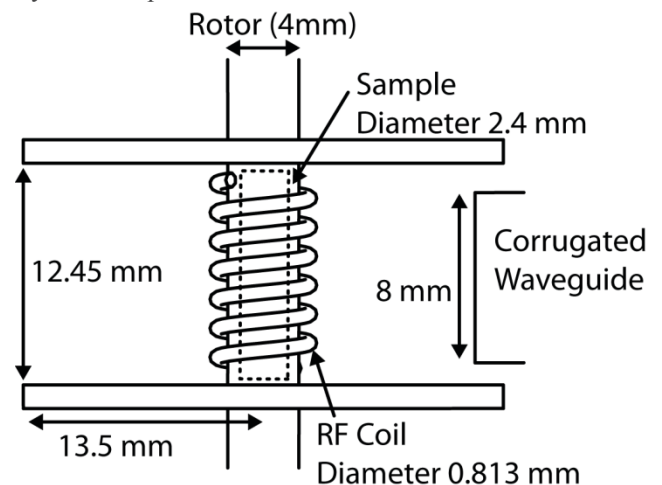


Figure 1: Cavity schematic of the HFSS model. The waveguide input launcher is on the right.

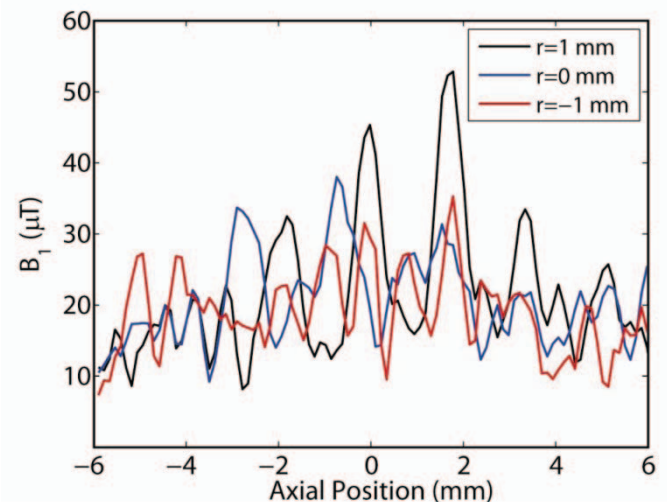


Figure 2: Axial profile of B_1 for 1 W coupled into the probe. The three curves correspond to different radial offsets from the sample axis and the plots are along the axis.

A precise value of B_1 was obtained using a full HFSS model of the sample chamber, as shown in Figure 1. The sample chamber is enclosed by a Kel-F cylinder with a radius of 13.5 mm and a height of 12.45 mm (not fully shown in Fig. 1). The Kel-F cylinder is partially coated with silver that reflects back some of the millimeter wave power, but its effectiveness is limited because power escapes through holes needed for rotor support and the high voltage leads of the RF pickup coil. The average B_1 value in the sample calculated using HFSS was 13.2 μT for an input power of 1 W. The axial distribution of B_1 can be seen in Figure 2 for three different radial locations within the sample. The peaks and nulls observed along the axis of the sample are the direct result of diffraction of the radiation as it passes through the closely spaced turns of the RF pickup coil. The non-uniform illumination of the sample by the Gaussian beam is evidenced by the much stronger B_1 values that are observed in the center of the sample.

The complex magnitude of the electric field in the cavity solved from the HFSS model is shown in Figure 3. Figure 3(a) is a cross section of the center of the probe along the symmetry axis of the rotor, Figure 3(b) is a cross section of the center of the probe perpendicular to the symmetry axis of the rotor. As shown in Figure 3, the standing wave in the input port of the probe is due to the large reflection from the RF pickup coil. The diffractive effect of the RF pickup coil produces peaks along the vertical axis of the rotor. Reflections produce some moding in the radial direction of the sample.

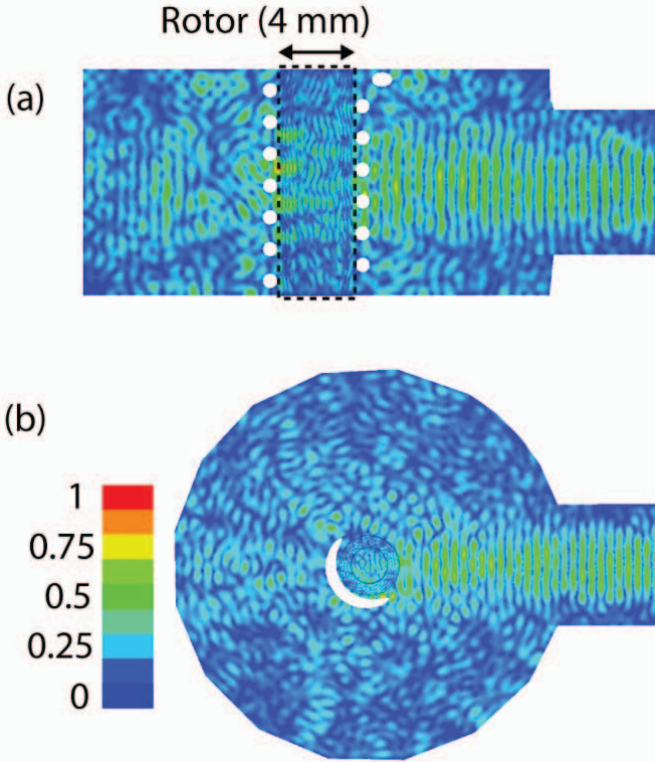


Figure 3: Complex magnitude of the electric field for the (a) vertical cross section of the probe, (b) the horizontal cross section of the probe. The white areas in (a) and (b) delimit the location of the metallic RF pickup coil.

III. SINGLE PASS MODEL

A single pass model was used as a simple, but approximate model of the DNP probe. Using this model, we were able to determine the effect that individual components in the sample cavity have on the millimeter wave coupling into the sample. The input corrugated waveguide launches a Gaussian beam into the probe that propagates through the RF pickup coil and sapphire rotor housing to the sample (Figure 1). The coil acts similar to a 2D metallic strip grating resulting in power transmission and reflection that depends strongly on the spacing-to-wavelength ratio.⁶ The power passing through the coil is highly diffracted when the coil spacing is comparable to the wavelength. The coil may also reflect a significant portion of the millimeter wave radiation. The radiation then passes through a sapphire rotor that acts as a converging lens and focuses the beam as it impinges on the sample. Using Gaussian beam optics and Fresnel diffraction, we obtained an approximate value of B_1 in the sample of 11 μT for an input power of 1 W. This model indicates that 25% of the radiated Gaussian beam power is not incident on the rotor and the transmission through the RF pickup coil is 40%. The calculated reflection coefficient for the vacuum-sapphire-sample boundary averaged over the incident angle produces 63% power transmission, resulting in a large fraction of the power being wasted. Some possibilities to address this will be mentioned later in the paper.

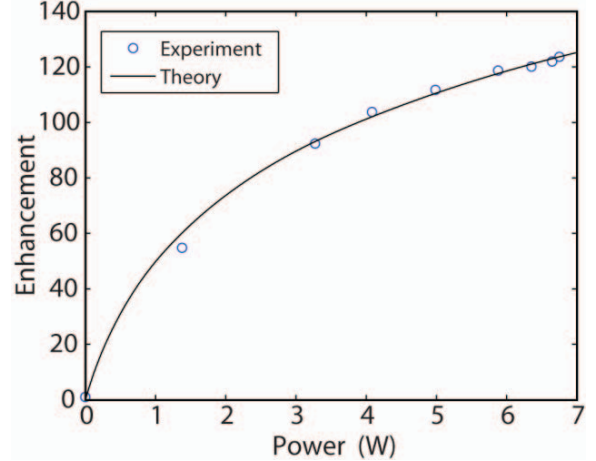


Figure 4: Enhancement curve for a fully packed rotor of 1 M ^{13}C -Urea dissolved in d_8 -glycerol/ $\text{D}_2\text{O}/\text{H}_2\text{O}$ (60%/30%/10% by volume).

IV. COMPARISON WITH EXPERIMENT

Knowing the B_1 field distribution in the sample allows one to calculate the change in signal enhancement that would be observed for differing sample cavity arrangements. It is crucial that a calculation of the signal enhancement takes into account the large variation in the intensity of the B_1 field in the sample. We calculate the total enhancement of the sample for a given field distribution by integrating the power dependence expression⁷ over the sample volume

$$\epsilon = \frac{1}{V} \int \epsilon_{\max} \left(\frac{\alpha B_1^2}{1 + \alpha B_1^2} \right) dV \quad (1)$$

where $\alpha = \gamma_e T_1 T_2$ from the expression of the Z magnetization from the Bloch equations, with $T_1 T_2 = 4 \times 10^{-12} \text{s}^2$ for 1 M ^{13}C -

Urea dissolved in d8-glycerol/D20/H₂O (60%/30%/10% by volume).⁸ The fit of this model to the data has excellent agreement and is shown in Figure 4. The measured and theoretical enhancement curves are plotted for the power delivered to the corrugated waveguide launcher shown in Figure 1.

To test the predictive ability of the B₁ field distribution generated by the HFSS simulations, the sample parameters found in Figure 4 were used to calculate the change in enhancement as a function of the rotor wall thickness. The layered dielectric medium produced by the sapphire-sample boundary of the cylindrical rotor should act as a low Q Fabry-Perot resonator that affects the transmission of the millimeter wave radiation into the sample. The outer diameter of the sapphire rotor is constrained to 4 mm by the bearings that support the rotor during sample rotation and the RF pickup coil. Therefore, the sample diameter is equal to 4 mm minus twice the rotor wall thickness. The predicted and measured enhancement values are shown in Figure 5. The enhancement was measured for four different rotor thicknesses using the same sample. The limited experimental data supports the theoretical calculations.

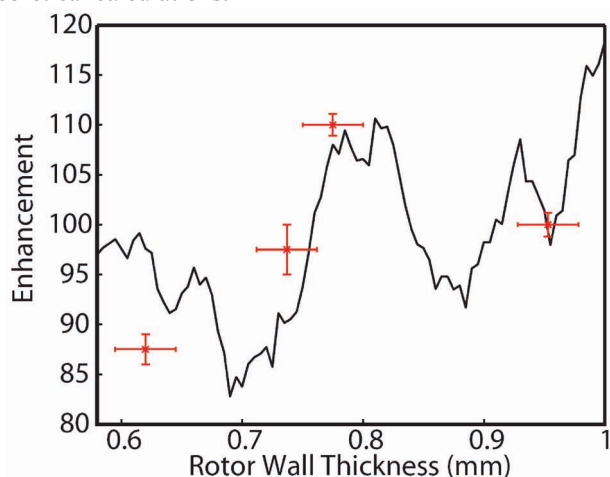


Figure 5: Enhancement vs. rotor wall thickness. Measured data are shown as dots with error bars.

V. DISCUSSION AND CONCLUSIONS

Although only a portion of the power produced from the millimeter wave source couples into the sample, the B₁ profile achieved in the sample is sufficient to reach satisfactory enhancement values. A more uniform distribution and improved coupling would produce higher enhancements. In comparison, electron paramagnetic resonance (EPR) and solution state DNP experiments are able to achieve higher average B₁ values per Watt of power and superior homogeneity. By using low order metallic resonant structures and sample volumes that occupy a small fraction of the resonator, B₁ values on the order of 1 mT/W^{1/2} have been reported.⁹ However, to optimize MAS DNP experiments, large sample volumes are required to maximize signal acquisition. Furthermore, rotating metallic components are not permissible in the sample chamber because they would attenuate the RF signal.

In addition to analyzing the current geometry of the probe, axial coupling into the sample, whereby the millimeter waves are launched along the axis, was also investigated. Besides the added difficulty of coupling into the sample from along the axis, the relatively high loss tangent will cause the 12.45 mm long sample to see a highly non-uniform illumination. For the present sample, the power transmitted through the sample along the sample axis would be only 33% of the incident power, producing a highly nonuniform B₁ profile. At higher frequencies, where the loss tangent and absorption coefficient are larger, this effect would be far worse. Furthermore, with such a large sample volume and high loss tangent, the addition of reflective end caps would have little impact.

Improvements to the sample cavity are currently being considered. The Gaussian beam that is launched into the sample cavity does not fully impinge on the surface area of the rotor, wasting a significant amount of power. A cylindrical dielectric lens made of Teflon could be used to focus the Gaussian beam perpendicular to the symmetry axis of the rotor, thereby increasing the incident power on the sample. The calculated average B₁ value in the sample with a lens increased to 14.3 μ T for an input power of 1 W. It is also possible to optimize the diameter-to-spacing ratio of the RF pickup coil to increase millimeter wave transmission into the sample. Adding a diffractive curvature to the lens along the axis of the sample is also being considered to provide a more uniform illumination. A uniform distribution of the B₁ field is desirable to maximize signal enhancement.

ACKNOWLEDGEMENTS

The authors gratefully acknowledge Ivan Mastovsky for his assistance. This work was supported by the NIH and NIBIB under Contracts EB001965 and EB004866.

REFERENCES

- [1] A. B. Barnes, et al., "High-Field Dynamic Nuclear polarization for Solid and Solution Biological NMR," *Appl. Magn. Reson.*, 2008, Vol. 34(3), pp. 237-263.
- [2] A. B. Barnes, et al., "Cryogenic Sample Exchange NMR Probe for Magic Angle Spinning Dynamic Nuclear Polarization," *Journal of Magn. Reson.*, 2009, Vol. 198(2), pp. 261-270.
- [3] P. P. Woskov, et al., "Corrugated Waveguide and Directional Coupler for CW 250-GHz Gyrotron DNP Experiments," *IEEE Trans. on Microwave Theory and Techniques*, 2005, Vol. 53(6), pp. 1863-1869.
- [4] J.H. Jiang, et al., "Ice and water Permittivities for Millimeter and Submillimeter Remote Sensing Applications," *Atmos. Sci. Let.*, 2004, Vol. 5, pp. 146-151.
- [5] J. Lamb, "Miscellaneous Data on Materials for Millimetre and Submillimetre Optics," *Int. Journal of Infrared and Millimeter Waves* 1996, Vol. 17(12), pp. 1997-2034.
- [6] W. Chambers, et al., "Freestanding Fine-Wire Grids for Use in Millimeter-and Submillimeter-Wave Spectroscopy," *Infrared and Millimeter waves: Electromagnetic Waves in Matter*, 1986, pp. 77.
- [7] B. Odintsov, et al., "Temperature Dependence of Solid-Liquid Scalar Interactions in Aqueous Char Suspensions by Nonstationary DNP at Low Magnetic Field," *Surface Science*, 1997, Vol. 393(1-3), pp. 162-170.
- [8] C. Farrar, et al., "Mechanism of Dynamic Nuclear Polarization in High Magnetic Fields," *The Journal of Chemical Physics*, 2001, Vol. 114, pp. 4922.
- [9] V. P. Denysnekov, et al., "High-Field DNP Spectrometer for Liquids", *Applied Magnetic Resonance*, 2008, Vol. 34(3), pp. 289-299.